

Cycle Slips in Phase-Locked Loops: A Tutorial Survey

GERD ASCHEID AND HEINRICH MEYR, MEMBER, IEEE

Abstract—Cycle slips in phase-locked loops are statistical, nonlinear phenomena. This makes a mathematical analysis extremely difficult. As a consequence, the results of such an analysis are not easily accessible to the practicing engineer.

It is the purpose of this survey paper to present a self-contained discussion of cycle slips in phase-locked loop avoiding advanced mathematical tools. Based on the results of an extensive experimental study we explain the underlying principle of the complex interaction between nonlinearity and noise. The results are complemented by simple, approximate analysis which agrees well with the experimental findings.

In addition, we present a new and complete set of diagrams on cycle slip statistics not presently available in the literature.

I. INTRODUCTION

MOST digital communication systems employ coherent demodulation techniques. This requires a receiver capable of accurately estimating the phase of the received signal.

The circuits for generating a carrier reference are all based on the same fundamental principle: a locally generated reference and the received signal are nonlinearly processed to generate an error signal which is subsequently used to adjust the phase of the VCO to that of the incoming signal. Consequently, this suggests that these synchronizers have the same mathematically equivalent baseband model shown in Fig. 1.

Depending on the particular modulation, different nonlinearities $g(\phi)$ and noise processes $n(t)$ will be obtained [2, p. 116].

The fact that there exists a common equivalent model is of great importance since it allows one to transpose the results obtained for the phase-locked loop (PLL) to more complex circuits such as Costas loops, etc.

Due to the noise, the VCO phase is a random process. When the VCO phase variance becomes large, a phenomenon occurs which is inherent to the nonlinearity in the loop. The VCO phase is increased to such an extent that the VCO slips one or several cycles with respect to the input phase. The occurrence of a slip is an event with very low probability for weak noise, but the probability increases steeply with increasing noise power. As an example, the cycle slipping rate of a first-order loop is plotted in Fig. 2 versus the loop signal-to-noise ratio ρ (which is defined in Section II). The same figure shows the phase variance $\sigma_{\hat{\theta}}^2$ obtained when the nonlinearity is taken into account and the phase variance σ_{lin}^2 when the linear

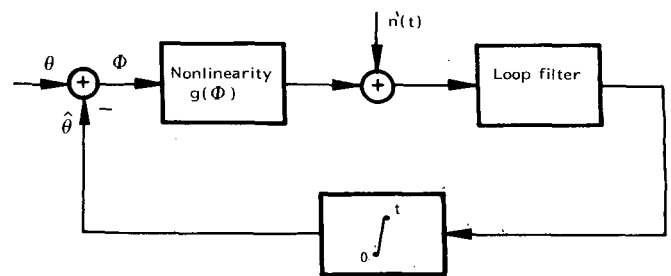


Fig. 1. Equivalent baseband model of synchronizers.

theory is used. While the departure of the variance $\sigma_{\hat{\theta}}^2$ from the linear theory is small, the slip rate varies by orders of magnitude within a small interval. A great deal of effort has been invested in the past in theoretical as well as experimental and computer simulation studies of cycle slips. Lindsey and Charles [10] presented results on experimental cycle slip distributions. Mean time between slips has been obtained by means of computer simulation in [11] and [12]. This short list is only a sampling of noteworthy papers. A comprehensive list on the subject can be found in the books on PLL's [1]-[5] and in a bibliography [13]. Lately, there has been a first commercial product announced which measures operating threshold based on slip rate [14].

The purpose of this paper is twofold:

- 1) to present a set of new experimental data on cycle slip rates and
- 2) to support these results with simple analyses in order to show the influence of the various loop parameters.

The main difference between the past work and this paper is that we examine the actual physical phenomenon of a cycle slip while the previous authors reported overall statistics (which is very important information).

In Section II a brief survey of well-known equations and results is given. We feel that such a survey is necessary because the definitions and notations in the PLL literature are not uniform. We have employed state variables since this is the only mathematical description that allows one to analyze the loop under nonlinear operating conditions. Normalized and dimensionless variables have been used. The main advantage of such a normalization is that the number of parameters is reduced to a few parameters having physical meaning.

Section III of the paper is entitled "Understanding Cycle Slips." We demonstrate that the state variable x_1 (proportional to the capacitor voltage in a second-order loop) is of utmost importance in understanding slips. For example, x_1 determines whether or not the cycle slips occur in bursts. Of great

Manuscript received November 1, 1981; revised March 22, 1982. This work was supported by the Deutsche Forschungsgemeinschaft (DFG) under Contract Me 651/3-3.

The authors are with Aachen Technical University, D-5100 Aachen, West Germany.

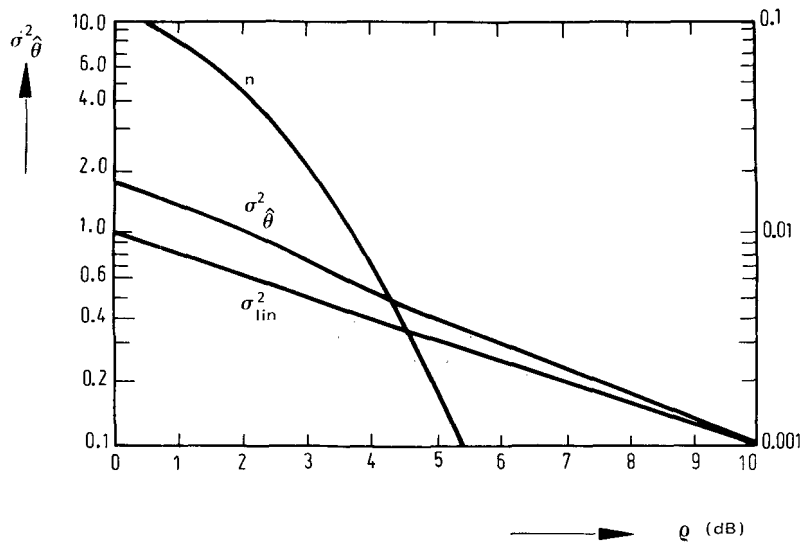


Fig. 2. Phase variance and normalized sliprate n as a function of the loop SNR ρ .

assistance, if not indispensable, in explaining the complicated interaction of noise and nonlinearity in a PLL, are trajectories for the phase error $\phi(t)$ and the other state variable $x_1(t)$ taken during a typical experiment. These trajectories, together with simple, approximate computations, allow one to obtain a good understanding of the influence the various parameters have on cycle slips.

In Section IV-A we give an overview of the experimental configuration. The experimental results are discussed in the next subsection. Finally, we briefly discuss the optimization of the loop parameters when the mean time between cycle slips is to be maximized.

II. LOOP EQUATIONS

A. Basic Equations and Definitions

We begin by recapitulating some well-known equations together with the notation to be used in the sequel. The material is covered in detail in any book on PLL's.

The input to the PLL equals the sum of signal $s(t)$ and noise $n(t)$

$$y(t) = s(t) + n(t) \tag{1}$$

where the signal $s(t)$ is given by

$$s(t) = \sqrt{2}A \sin(\omega_0 t + \theta) \tag{2}$$

and $n(t)$ is a narrow-band Gaussian noise process

$$n(t) = \sqrt{2}n_c(t) \cos \omega_0 t + \sqrt{2}n_s(t) \sin \omega_0 t. \tag{3}$$

The features of this process together with the definition of equivalent noise bandwidth B_{IF} of an IF-filter preceding the PLL and the signal-to-noise ratio at the output of the IF-filter are summarized in Table I(a).

We model the phase detector as an ideal multiplier. The output of the multiplier in Fig. 3(a) equals (double frequency terms are neglected)

$$\epsilon(t) = K_D [\sin \phi(t) + n'(t)] \tag{4}$$

with

$$K_D = K_m K_1 A \tag{V}$$

$$\sqrt{2}K_1 = \text{amplitude of VCO-signal} \tag{V}$$

$$K_m = \text{multiplier gain} \tag{V^{-1}}$$

$$\theta = \text{phase of input signal}$$

$$\hat{\theta} = \text{phase of VCO}$$

$$\phi = \theta - \hat{\theta} = \text{phase error}$$

and

$$n'(t) = \frac{n_c(t)}{A} \cos \hat{\theta} + \frac{n_s(t)}{A} \sin \hat{\theta}. \tag{5}$$

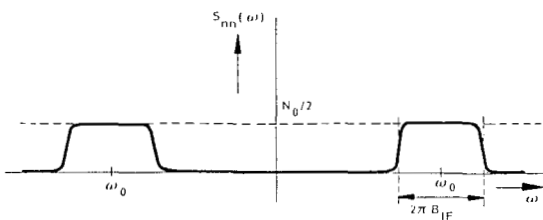
An exact equivalent circuit of the phase detector is shown in Fig. 3(b) and the power spectrum of $n'(t)$ is shown in Table I(b).

Under the assumption of small phase error the PLL has the mathematically equivalent model shown in Fig. 4. The variance $\sigma_{\hat{\theta}}^2$ of the output phase due to the noise disturbance $n'(t)$ is

$$\sigma_{\hat{\theta}}^2 = \frac{1}{2\pi} \int_{-\infty}^{+\infty} |H(\omega)|^2 S_{n'n'}(\omega) d\omega \tag{6}$$

with the loop transfer function

TABLE I(a)
POWER SPECTRUM OF THE NOISE PROCESS $N(T)$



$$S_{nn}(\omega) = |F_{IF}(\omega)|^2 \frac{N_0}{2}$$

$F_{IF}(\omega)$: IF filter spectrum,
 $|F_{IF}(\pm\omega_0)| = 1$

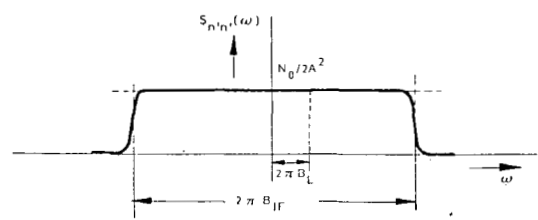
Equivalent bandwidth: $B_{IF} = \frac{1}{2\pi} \int_0^\infty |F_{IF}(\omega)|^2 d\omega$

Noise power: $P_N = \frac{1}{2\pi} \int_{-\infty}^\infty S_{nn}(\omega) d\omega = N_0 B_{IF}$

Signal power: $P_S = A^2$

Signal-to-noise ratio: $SNR_i = \frac{P_S}{P_N} = \frac{A^2}{N_0 B_{IF}}$

TABLE I(b)
PHASE DETECTOR OUTPUT



Noise power spectrum $S_{n'n'}(\omega)$

Noise variance: $\sigma_{n'}^2 = \frac{N_0 B_{IF}}{2A^2} = \frac{1}{2SNR_i}$

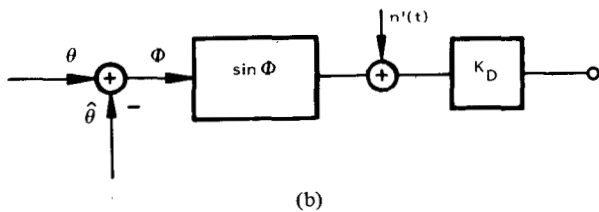
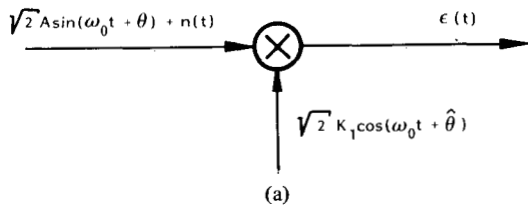


Fig. 3. (a) Multiplier type phase detector. (b) Mathematically equivalent model of the phase detector.

$$H(\omega) = \frac{K_0 K_D F(s)/s}{1 + K_0 K_D F(s)/s} \Big|_{s=i\omega} \quad (7)$$

$F(s)$: loop filter.

The equivalent loop bandwidth B_L is defined as,

$$B_L = \frac{1}{2\pi} \int_0^{+\infty} |H(\omega)|^2 d\omega \quad [\text{Hz}]. \quad (8)$$

If the equivalent noise bandwidth B_L is much smaller than the bandwidth B_{IF} , the loop "sees" a white noise process with constant power spectral density (Table I):

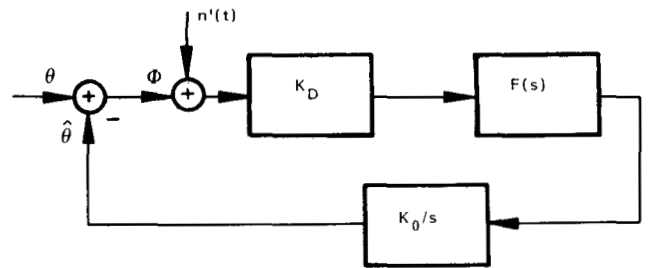


Fig. 4. Equivalent linearized baseband model of the phase-locked loop.

$$S_{n'n'}(\omega) = \frac{N_0}{2A^2}. \quad (9)$$

Inserting (8) and (9) into (6) yields

$$\sigma_{\theta}^2 = \frac{N_0 B_L}{A^2} \quad [\text{rad}^2]. \quad (10)$$

The inverse variance is often called signal-to-noise ratio in the loop and given the symbol ρ .

$$\rho = \frac{1}{\sigma_{\theta}^2} = \frac{A^2}{N_0 B_L}. \quad (11)$$

Using signal and noise power, (11) can be rewritten

$$\rho = \frac{P_S}{P_N} \cdot \frac{B_{IF}}{B_L} = SNR_i \cdot \frac{B_{IF}}{B_L}. \quad (12)$$

This form is particularly well suited for measurement. The definition of ρ is not unique in the PLL literature. In the form (11) it is used by Lindsey [2], Viterbi [3], and Blanchard [4]. Gardner [5, p. 32] has a factor of 0.5 in his definition. His definition is equally arbitrary and is as valid as ours.

B. State Variable Description of the Second-Order PLL

To describe and understand the nonlinear behavior of the phase-locked loop we need a state variable description. For the second-order PLL with loop filter (Fig. 5)

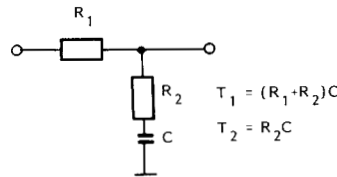


Fig. 5. Loop filter of a second-order PLL with imperfect integrator (lag-lead filter).

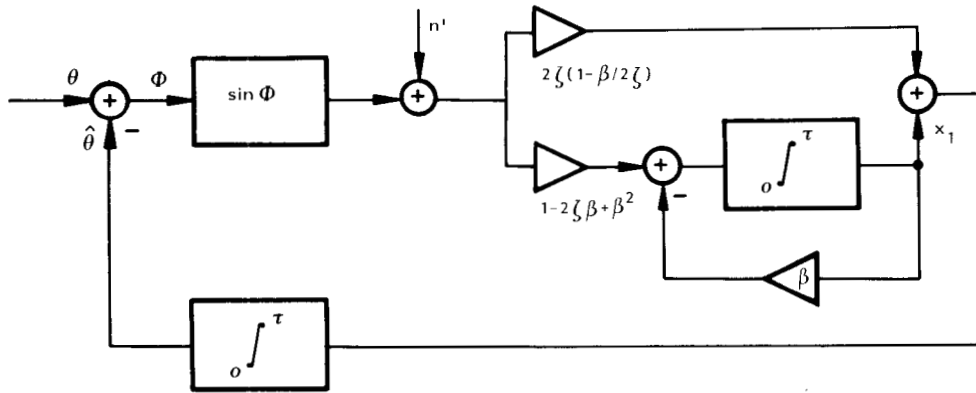


Fig. 6. Equivalent model of a second-order PLL with imperfect integrator using normalized variables.

$$F(s) = \frac{1 + sT_2}{1 + sT_1} = \frac{T_2}{T_1} + \frac{1 - T_2/T_1}{1 + sT_1} \tag{13}$$

the nonlinear differential equations are

$$\begin{aligned} \frac{d\phi}{dt} &= -K_0 \frac{T_2}{T_1} K_D [\sin \phi + n'] - y_1 + \frac{d\theta}{dt} \\ \frac{dy_1}{dt} &= -\frac{1}{T_1} y_1 + \frac{1 - T_2/T_1}{T_1} \cdot K_0 K_D [\sin \phi + n']. \end{aligned} \tag{14}$$

The state variable $y_1(t)$ is proportional to the capacitor voltage $u_c(t)$ of the loop filter

$$y_1(t) = K_0(1 - T_2/T_1)u_c(t) \tag{15}$$

and has the physical dimension of angular frequency.

The state equations as they stand are of little value. The parameters can vary over orders of magnitude; their influence on loop performance is hard to oversee. Introducing appropriate normalized and dimensionless variables yields a set of equations with parameters more easily interpreted. We introduce the normalized time τ and replace y_1 by the dimensionless quantity x_1 as follows:

$$\tau = \omega_n \cdot t \quad x_1 = \frac{y_1}{\omega_n} \quad \beta = \frac{\omega_n}{K_0 K_D} \tag{16}$$

Using the definitions of the natural frequency ω_n and the loop damping factor ζ

$$\omega_n = \sqrt{\frac{K_0 K_D}{T_1}} \quad \zeta = \frac{1}{2} \omega_n \left[T_2 + \frac{1}{K_0 K_D} \right] \tag{17}$$

we arrive, after some algebraic manipulations, at

$$\begin{aligned} \frac{d\phi}{d\tau} &= -2\zeta \left[1 - \frac{\beta}{2\zeta} \right] \sin \phi - x_1 - 2\zeta \left[1 - \frac{\beta}{2\zeta} \right] n' + \frac{d\theta}{d\tau} \\ \frac{dx_1}{d\tau} &= -\beta x_1 + [1 - 2\zeta\beta + \beta^2] \sin \phi \\ &\quad + [1 - 2\zeta\beta + \beta^2] n'. \end{aligned} \tag{18}$$

A mathematically equivalent model of the PLL using the normalized variables is shown in Fig. 6.

In (18) only the two parameters, loop damping ζ and the frequency ratio β , appear (aside from the natural frequency ω_n absorbed in τ). The reader will notice the use of ω_n and ζ in a nonlinear state equation. These quantities are formally defined in the same way as for a linear system.

The values of practical interest of ζ lie in the range of $0.5 < \zeta < 5$. We can also delimit values for β . The ratio T_2/T_1 is given by

$$\frac{T_2}{T_1} = \beta(2\zeta - \beta) > 0. \tag{19}$$

From (19) we find

$$0 < \beta < 2\zeta. \tag{20}$$

In the case of the commonly used high-gain loop we have $\beta \ll 1$, typically $0.001 \leq \beta \leq 0.1$. If we formally set $\beta = 0$ we obtain the equations for the second-order loop with perfect loop integrator. For reasonably small β the dynamic behavior for the imperfect second-order loop is practically indistinguishable from the perfect integrator loop with $\beta = 0$. In most of

our discussions on cycle slips we set $\beta = 0$ for simplicity. There is one important difference, however, in the steady state. In the noise free case the state variables assume the values

$$\phi = \sin^{-1} \left(\frac{\Delta\omega}{\omega_n} \cdot \beta \right)$$

$$x_1 = \frac{\Delta\omega}{\omega_n} (1 - 2\zeta\beta + \beta^2). \quad (21)$$

The loop with perfect integrator compensates a (normalized) frequency difference $\Delta\omega/\omega_n$ with a value of the integrator output x_1 of exactly $\Delta\omega/\omega_n$. The steady state phase error ϕ is zero. With an imperfect integrator there always exists a static phase error which substantially increases the cycle slip rate as will be seen in a later section of this paper.

III. UNDERSTANDING CYCLE SLIPS

We already know from Fig. 2 that the cycle slip rate is extremely dependent on the signal-to-noise ratio. As will be shown presently, the damping factor ζ also has a strong influence on the slip rate as well as on the manner of occurrence of the slips.

In Fig. 7 the probability that the time between two slips T_s is shorter than t is plotted for two values of ζ . For $\zeta = 0.24$ we observe a steep increase in $P(T_s < t)$ for small t , i.e., many slips have a very short duration compared to the mean time between slips. This means that the slips occur in bursts: if viewed on an oscilloscope we see clusters of slips of very short duration separated from each other by long time intervals.

For large damping, the distribution $P(T_s < t)$ is virtually exponential. From probability theory we know that exponentially distributed times between events imply statistical independence of these events. We therefore conclude that the cycle slips are independent, isolated events for large damping.

Having recognized the burst-like appearance of slips for small damping factors and the isolated event structure for large damping, we presently want to explain this different behavior.

A. Loops with Small Damping Factors

In Fig. 8 we have plotted an example of phase error ϕ and state variable x_1 as a function of normalized time τ for $\zeta = 0.24$ and a very small SNR. We clearly recognize the burst-like nature of the cycle slips. Before we turn our attention to the bursts of cycle slips we examine the behavior of the loop between two bursts, i.e., in its tracking mode. A damping of $\zeta = 0.24$ means that in the tracking mode (where linearization applies), we expect to observe a weakly damped oscillation of $\phi(\tau)$ and $x_1(\tau)$ sustained by the noise process $n'(\tau)$.

The average period of this oscillation is

$$\tau_p = \frac{2\pi}{\sqrt{1-\zeta^2}} = 6.67 \quad (22)$$

in normalized time. From Fig. 8 we find an average period of 7, which is not far from the predicted number. We would also

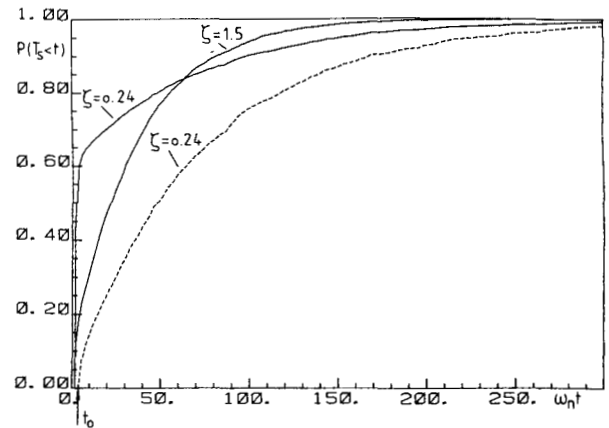


Fig. 7. Probability distribution $P(T_s < t)$ (solid lines) of the time between slips and conditional distribution $P(T_s < t | T_s > t_0)$ (dashed line), conditioned on the fact that T_s exceeds a given time t_0 . Signal-to-noise ratio $\rho = 2$ (numeric ratio).

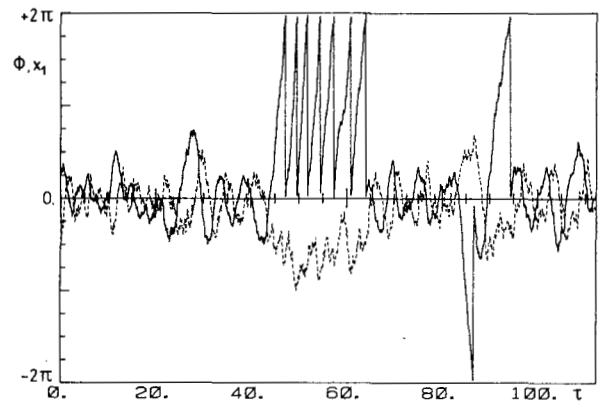


Fig. 8. Trajectories of phase error $\phi(\tau)$ and state variable $x_1(\tau)$ versus normalized time for $\beta = 0.03$, $\zeta = 0.24$, and $\rho = 2$ (numeric ratio).

expect an oscillation of $x_1(\tau)$ with the same period as ϕ but shifted by $\pi/2$, and this is indeed found in Fig. 8. To go one step further, x_1 and ϕ must have approximately the same amplitude, because of the normalizations that have been performed. For x_1 and ϕ we read off from Fig. 8 a value of 1; converting the average amplitude of ϕ into degrees gives approximately 60° .

The weaker the noise, the smaller the amplitude of $x_1(\tau)$ and $\phi(\tau)$ since the weak noise can push the loop only slightly away from its stable equilibrium. From linear theory we know $\sigma_\phi^2 = 1/\rho$; hence, the amplitude of the perturbed sinusoid would be $\sqrt{2/\rho}$. For strong noise, as in Fig. 8, it is very probable that the amplitude of the fluctuations exceeds the 90° phase error (maximum restoring force), in which case a cycle slip is very likely to occur. Furthermore, in this case the $x_1(\tau)$ variable follows to a wrong value. After completion of the first cycle slip, $x_1(\tau)$, which is responsible for frequency correction, has a wrong initial value (loop stress) and, consequently, is much more susceptible to another cycle slip.

The experimentally determined average value of x_1 taken at the completion of a cycle slip as a function of ρ is shown in Fig. 9(a). Indicated in this figure are the normalized pull-out frequency given by [5]

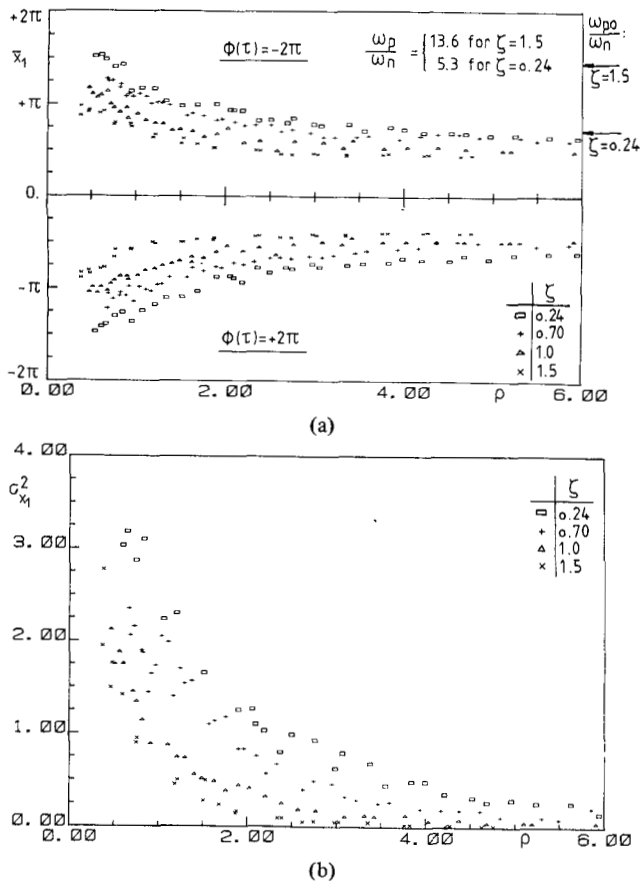


Fig. 9. (a) Conditional experimental mean \bar{x}_1 of the state variable $x_1(\tau)$, taken at the instant $\phi(\tau) = \pm 2\pi$ (completion of a cycle slip). (b) Conditional experimental variance $\sigma_{x_1}^2 = \overline{(x_1 - \bar{x}_1)^2}$ taken at the completion of a cycle slip.

$$\frac{\omega_{p0}}{\omega_n} = 1.8(1 + \zeta) \tag{23}$$

and the pull-in frequency [5] of the second-order loop with imperfect integrator

$$\frac{\omega_p}{\omega_n} = 2 \sqrt{\frac{\zeta}{\beta}} \tag{24}$$

If the loop starts with zero phase error $\phi(0) = 0$, then $x_1(0) = \omega_{p0}/\omega_n$ is the maximum initial frequency deviation for which the loop does not skip one or more cycles but remains in lock. The pull-in frequency is the maximum frequency difference for which the loop will lock, eventually, after a long acquisition period. Both frequencies hold for the noise-free case only, but serve as a good indicator for the noisy case.

For a small damping factor the average value of x_1 is—even for large SNR—only slightly smaller than the pull-out frequency. This means that a burst of cycle slips rather than a single cycle slip is to be expected. For $\rho < 5$ (7.0 dB) and $\zeta = 0.24$ the average of x_1 is larger than the pull-out frequency and a single cycle slip is very unlikely. In addition, the larger the difference $|x_1 - \omega_{p0}/\omega_n|$, the longer the mean duration of the burst will be.

The average of x_1 as a function of ρ increases rapidly with decreasing ρ , see Fig. 9(a). For $\rho = 1$ (0 dB) x_1 has come very close to the pull-in frequency of the loop. Since the experimental variance $\sigma_{x_1}^2$ [Fig. 9(b)] taken at the completion of a cycle slip also increases with decreasing ρ , it is very likely that x_1 assumes a value larger than the pull-in frequency once the loop has started slipping cycles. Therefore, once the loop has lost lock it stays out of lock with high probability. Control of the VCO is lost and its frequency wanders off from the signal frequency. This phenomenon has been called drop-lock in the literature. Actually, there is no well-defined noise threshold below which the PLL falls out and stays out of lock; there is no fundamental difference between repeated cycle slips and drop of lock (but see Section III-C on loop detuning).

The wandering off of the VCO at extremely low SNR is easily explained if we recognize that the restoring force in the equivalent model of Fig. 6 can be neglected, if x_1 is larger than the pull-in frequency. But neglecting the restoring force $\sin \phi$ is equivalent to opening the feedback system (see Fig. 6). In this case, the input to the integrator representing the VCO consists of the noise process plus $x_1(\tau)$. As is well known, the variance of an integrated noise process increases with τ ; hence, it is unbounded and the VCO wanders off.

It is very instructive to examine loop behavior during a burst of slips. We want to examine in detail the first, the last, and a cycle in the middle of a burst. Examples of bursts having the same parameters are shown in Fig. 10 and in expanded scale in Fig. 11 and Fig. 12.

Due to noise, the magnitude of both the phase error $\phi(\tau)$ and of $x_1(\tau)$ increase at the beginning of the first cycle slip [Fig. 11, region (a)]. (To correct the negative going phase error $x_1(\tau)$ should become negative.) The phase error passes through $-\pi/2$, the point of maximum restoring force toward $-\pi$. In the interval of $-\pi \leq \phi \leq -2\pi$, the restoring force has the wrong polarity; there is positive feedback in the loop. Since $x_1 > 0$, the phase error rapidly passes this region of positive feedback to reach $\phi = -2\pi$, which, of course, is equivalent to zero phase error. At completion of the first slip, $x_1(\tau)$ assumes a random value of slightly more than the pull-out frequency. During the following three cycle slips the value of x_1 increases to a maximum before it is slowly decreased to its correct average value of $x_1 = 0$. Another burst is shown in Fig. 12. In contrast to the previous burst we do not observe a pumping up of the x_1 variable during the first cycle slips. Rather, the value of x_1 , taken at the completion of a cycle slip, fluctuates around the experimental mean value x_1 before it takes on a value $x_1 < \omega_{p0}/\omega_n$, such that the loop can pull in.

Looking at the two (entirely different) bursts, the question arises whether we have observed examples of two different phenomena or whether there exists a common mechanism in both cases. We will see that there indeed exists a common mechanism in both cases consisting of a systematic force driving the PLL towards its stable equilibrium and a random perturbation. We will first analyze the force and later on compute the variance of the random perturbation.

A typical cycle in the middle of a burst is shown in region (b) of Fig. 11. It is typical, in the sense that a value $x_1(\tau)$

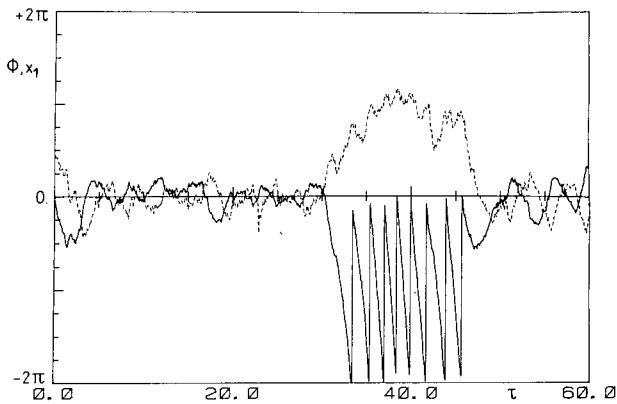


Fig. 10. Typical burst of a weakly damped ($\zeta = 0.24$) second-order loop. Signal-to-noise ratio $\rho = 3$ (numeric ratio).

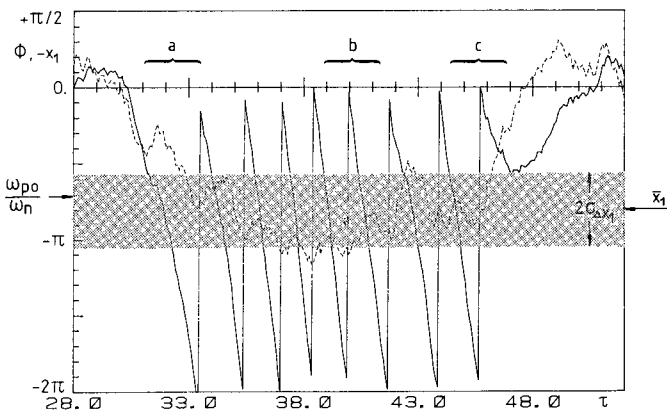


Fig. 11. Part of the trajectory of Fig. 10 in expanded scale. Note that $-x_1(\tau)$ is displayed.

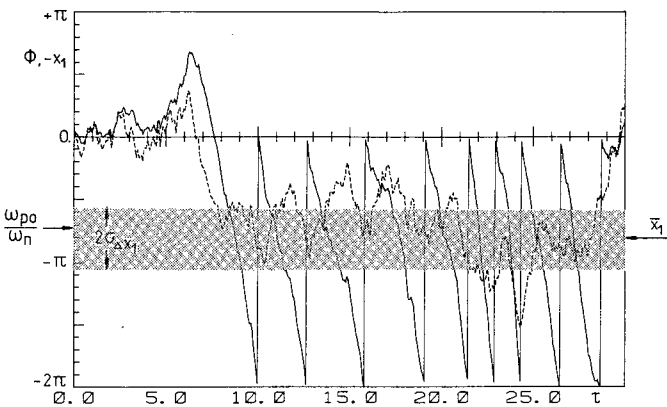


Fig. 12. Part of another trajectory with the same parameters as in Fig. 10. Note that $-x_1(\tau)$ is displayed.

exists which is erroneously interpreted by the PLL as a frequency detuning. Looking a little closer at this cycle slip, we notice that the phase error traverses the region $-\pi \leq \phi \leq -2\pi$ faster than the interval from $[0, -\pi]$. Since the restoring force $\sin \phi$ has the correct polarity within the interval $\tau_{bn}^+ = [0, -\pi]$, the absolute value of $x_1(\tau)$ as the integral of $\sin \phi$ is decreased. Within the interval $\tau_{bn}^- = [-\pi, -2\pi]$, however, the restoring force has the wrong polarity and instead of reducing $|x_1(\tau)|$ it moves it further away from the correct value $x_1(\tau) = 0$. Since, however, the interval τ_{bn}^- is shorter than τ_{bn}^+ , there is a net gain. To get a feeling for this net gain, we make an approximate computation.

Let us assume x_1 to be constant and neglect the noise $n'(\tau)$. The loop is then governed by the differential equation

$$\frac{d\phi}{d\tau} = -2\zeta \sin \phi - x_1. \tag{25}$$

Equation (25) is the differential equation of a first-order loop with frequency detuning $\Delta\omega = x_1$. If $x_1 > 2\zeta$, the loop will not lock but produce a periodic oscillation called beat note. In Fig. 13 we have shown the phase error $\phi(\tau)$ and the phase detector output $\sin \phi(\tau)$.

The periodic waveform $\sin \phi(\tau)$ is not symmetric but has a dc-component that can be obtained by integrating the differential equation over a full cycle.

$$\phi(\tau_{bn}) - \phi(0) = -2\zeta \int_0^{\tau_{bn}} \sin \phi(\tau) d\tau - x_1 \tau_{bn}. \tag{26}$$

Since $\phi(\tau_{bn}) = -2\pi$ and $\phi(0) = 0$ we obtain

$$\overline{\sin \phi} = \frac{1}{\tau_{bn}} \int_0^{\tau_{bn}} \sin \phi d\tau = -\frac{x_1}{2\zeta} + \frac{2\pi}{2\zeta \tau_{bn}} \tag{27}$$

$(x_1 > 0, \text{ negative cycle slip}).$

By standard separation of variable techniques [2] the beat note period is found to be

$$\tau_{bn} = \frac{\pi}{\zeta} \cdot \frac{1}{\sqrt{\left(\frac{x_1}{2\zeta}\right)^2 - 1}} \cong \frac{2\pi}{|x_1|} \cdot \frac{1}{1 - \frac{1}{2}\left(\frac{2\zeta}{x_1}\right)^2}; \tag{28}$$

$\left(\frac{2\zeta}{x_1}\right)^2 \ll 1.$

Inserting (28) into (27) yields

$$\overline{\sin \phi} = -\frac{\zeta}{x_1}. \tag{29}$$

Note that a positive value of x_1 produces a negative dc-term $\sin \phi$ and vice versa. It is exactly this dc-term that is integrated in the loop filter of a second-order loop and reduces $x_1(\tau)$ to its correct value of $x_1(\tau) = 0$, thereby pulling the PLL back into its tracking range. The accumulated voltage during one cycle is

$$\overline{\Delta x_1} \cong \overline{\sin \phi} \cdot \tau_{bn} = -\frac{2\pi\zeta}{|x_1| |x_1|}; \quad (|x_1| \gg 2\zeta). \tag{30}$$

The noise process n' causes a random (mean free) fluctuation of the increment Δx_1 . Under the same approximation as in (30) the random increment Δx_1 equals the integral of the white noise process $n'(\tau)$ over $[0, \tau_{bn}]$:

$$\Delta x_1(\tau_{bn}) = \int_0^{\tau_{bn}} n'(\tau) d\tau. \tag{31}$$

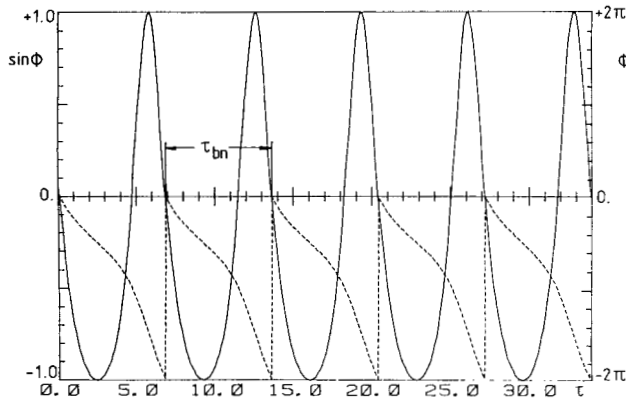


Fig. 13. Phase error $\phi(\tau)$ and phase detector output $\sin \phi(\tau)$ during a beatnote.

The variance of this increment is easily found to be

$$\sigma_{\Delta x_1}^2 \cong \frac{4\zeta}{1 + (2\zeta)^2} \frac{1}{\rho} \frac{2\pi}{|x_1|} \tag{32}$$

The mean value $\overline{\Delta x_1}$ in (30) can be interpreted as systematic drift force while the variance $\sigma_{\Delta x_1}^2$ describes a random diffusion. For the data given in Fig. 11 and a value of $x_1 = 2.5$ we obtain for $\overline{\Delta x_1}$, $\sigma_{\Delta x_1}$, and for τ_{bn}

$$\tau_{bn} = 2.8 \quad \overline{\Delta x_1} = 0.24 \quad \sigma_{\Delta x_1} = 0.81. \tag{33}$$

The random fluctuation is much larger than the systematic driving force $\overline{\Delta x_1}$. The different appearance of the two bursts is now easily understood. The systematic force $\overline{\Delta x_1}$ is covered by the random fluctuations; the values of x_1 taken at the completion of a cycle slip are within a band of $2\sigma_{\Delta x_1}$ width, centered around $\overline{x_1}$. What looks like a systematic pumping up effect in Fig. 11 is nothing but a normal statistical fluctuation.

Our simple analysis is only approximate but predicts, remarkably well, the duration of a slip within a burst as well as the statistical fluctuations of the increment $\overline{\Delta x_1}$.

The distinctive features in region (c) are that the cycle slipping stops and x_1 rapidly converges toward zero. Immediately after the last cycle slip, the phase error rapidly increases. The restoring force $\sin \phi$ is large and has the correct polarity during the convergence interval. Integration of the restoring force proceeds rapidly so that x_1 quickly moves toward zero.

In passing, formulas (30) and (32) give a hint as to why the loop permanently loses lock for decreasing ρ . The average pull-in effect $\overline{\Delta x_1}$ is inversely proportional to $(x_1)^2$, while the variance is inversely proportional to ρ and x_1 . From Fig. 9(a) we know that the average $\overline{x_1}$ increases for decreasing ρ . Therefore, the bursts tend to become longer until the loop eventually loses lock completely.

B. Overdamped Loops ($\zeta > 1$)

Having understood the rather complex structure of the cycle slips of an underdamped loop we turn our attention to loops having damping factors $\zeta > 1$. As already noted, cycle slips occur in this case as isolated events, not in bursts. Why this difference?

The answer is again found by inspection of $\overline{x_1}$ in Fig. 9(a). We first note that $\overline{x_1}$ is, for reasonably large ρ , less than 1/3 of the pull-out frequency. Secondly, the function $\overline{x_1}(\rho)$ is essentially flat for $\rho > 4$. It remains for all ρ much smaller than the pull-out frequency ω_{p0}/ω_n (not to mention the pull-in range ω_p/ω_n). From this and the variance $\sigma_{x_1}^2$ in Fig. 9(b) it is clear that bursts of cycle slips are extremely unlikely events. The mean time between cycle slips converges for low ρ toward the values of a first-order loop which always performs better than a second-order loop, provided there is no frequency difference between VCO and signal.

We still owe an explanation as to why the variable x_1 takes on such small values. As always, linear theory is instrumental in getting a good understanding of the nonlinear behavior.

A large damping implies a large time constant for the x_1 -integrator; the response of such an integrator to a noise event is very sluggish and small in amplitude. Therefore, the proportional path of the filter determines the short-time transients while the integral path compensates for an eventual frequency difference between VCO and signal. Thus, for the computation of the short-time transients of $\phi(\tau)$ we may approximately assume x_1 to be constant. But the input to the integrator of the loop filter equals the input to the $\hat{\theta}(\tau)$ -integrator, if multiplied by $1/2\zeta$. Hence, the increments of x_1 and θ are approximately equal:

$$x_1(\tau) - x_1(0) \cong \frac{1}{2\zeta} (\hat{\theta}(\tau) - \hat{\theta}(0)). \tag{34}$$

Since $\hat{\theta}(\tau) = -\phi(\tau)$ we may write

$$x_1(\tau) - x_1(0) \cong -\frac{1}{2\zeta} (\phi(\tau) - \phi(0)) \tag{35}$$

for the short-time transients.

A typical cycle slip is displayed in Fig. 14. We observe a very similar shape of $x_1(\tau)$ and $\phi(\tau)$ up to the end of the cycle slip. Subsequently, the value of $x_1(\tau)$ slowly decreases to its initial value of $x_1(\tau) = 0$ with a time constant of 2ζ , corresponding to the neglected pole of the second-order loop. Note, however, that $\phi(\tau)$ after the slip is much less affected by $x_1(\tau)$.

Having recognized the similarity of $x_1(\tau)$ and $\phi(\tau)$ [as predicted by (35)] we are in a position to compute an estimate of $x_1(\tau)$ at the completion of a cycle slip. Let us denote by τ_0 and $\tau_{2\pi}$, the beginning and end of a cycle slip, respectively, and define a cycle slip as part of the trajectory $\phi(\tau)$ such that $\phi(\tau_0) = 0$ and $\phi(\tau \leq \tau_{2\pi}) \neq 0$. Furthermore, we assume $x_1(\tau_0) = 0$. Under these assumptions we obtain for $x_1(\tau_{2\pi})$

$$x_1(\tau_{2\pi}) = \int_{\tau_0}^{\tau_{2\pi}} [\sin \phi(\tau) + n'(\tau)] d\tau \tag{36}$$

$\tau_{2\pi} - \tau_0$: random variable.

Neglecting the integral path of the loop filter for the short-time interval $(\tau_{2\pi} - \tau_0)$, the PLL is governed by a first-order differential equation

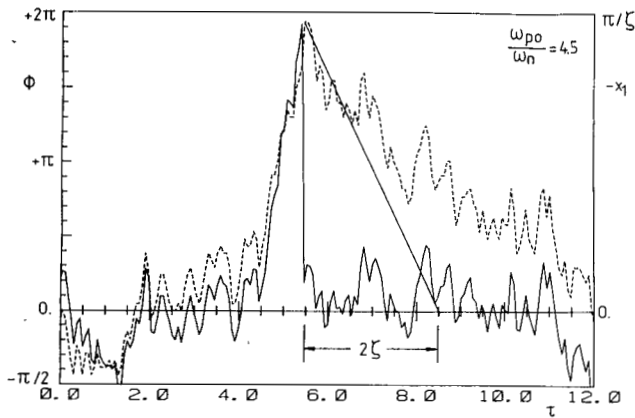


Fig. 14. Cycle slip of an overdamped loop ($\zeta = 1.5$) for $\rho = 2.5$ (numeric ratio). Note that $-x_1(\tau)$ is displayed.

$$\frac{d\phi}{d\tau} = -2\zeta [\sin \phi(\tau) + n'(\tau)]. \quad (37)$$

Note that the right-hand side of (37) multiplied by $-1/2\zeta$ equals the integrand in (36). Integration of the stochastic differential equation (37) from τ_0 to $\tau_{2\pi}$ yields

$$\phi(\tau_{2\pi}) - \phi(\tau_0) = -2\zeta \int_{\tau_0}^{\tau_{2\pi}} [\sin \phi(\tau) + n'(\tau)] d\tau \quad (38)$$

but $\phi(\tau_0) = 0$ and $|\phi(\tau_{2\pi})| = 2\pi$, by definition. Replacing the right-hand side of (36) by $-\phi(\tau_{2\pi})/2\zeta$ yields

$$x_1(\tau_{2\pi}) = \begin{cases} \pi/\zeta \text{ negative cycle slip,} & \phi(\tau_{2\pi}) = -2\pi \\ -\pi/\zeta \text{ positive cycle slip,} & \phi(\tau_{2\pi}) = +2\pi. \end{cases} \quad (39)$$

As in the case of small damping factors ζ , $x_1(\tau_{2\pi})$ appears as a frequency detuning. However, the detuning is too small compared to the pull-out range to produce a burst. The inverse dependence of $x_1(\tau_{2\pi})$ is experimentally well confirmed; see Fig. 9. Due to the coupling of $x_1(\tau)$ and $\phi(\tau)$, the result (39) is, of course, only an approximation.

So far we have discussed two examples of loops of $\zeta = 0.24$ and $\zeta = 1.5$ damping and have found a tendency that weakly damped loops burst while overdamped loops do not. It would be interesting to identify a boundary between bursting and nonbursting. Of course, such a boundary cannot be a rigid one, but would merely provide information as to whether a loop is more likely to burst or not.

On the average, a loop will burst only if the mean value of x_1 taken at the completion of the slip is larger than the pull-out frequency. Using (39) and (23) yields the inequality

$$\pi/\zeta > 1.8(1 + \zeta) \quad \text{condition for burst.} \quad (40)$$

Solving (40) we find that loops with damping factors of $\zeta < 0.9$ will burst.

C. Frequency Detuning

A frequency difference $\Delta\omega$ between sender and receiver causes a static phase error; the x_1 variable assumes a value of $x_1 = \Delta\omega/\omega_n$ in order to compensate for the frequency dif-

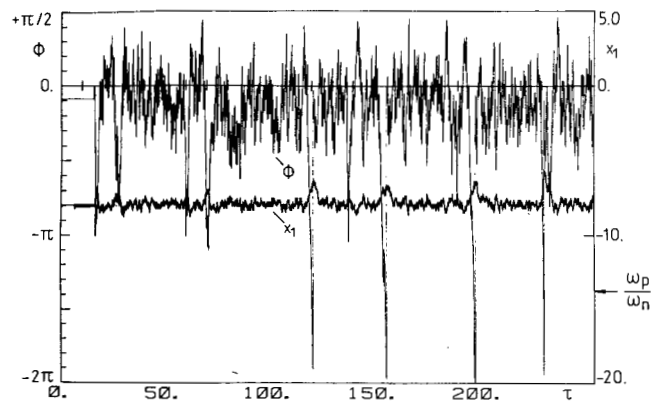


Fig. 15. Trajectories $\phi(\tau)$ and $x_1(\tau)$ of a second-order loop with $\zeta = 1.0$ and $\rho = 2.8$ and a loop stress of $\Delta\omega/\omega_n = 8$.

ference as shown by example in Fig. 15. Because the difference between maximum restoring force and the stable equilibrium point is reduced to $1 - \sin(\beta\Delta\omega/\omega_n)$, the loop slips much more often to this side than would be the case for zero detuning.

In the experiment, it was observed that if $\Delta\omega/\omega_n$ was increased above the pull-in range, the loop, with very high probability, completely lost lock after once slipping a cycle, a behavior not observed for the same signal-to-noise ratio with zero detuning.

To discuss this phenomenon, a few preliminary remarks are helpful. In the noise-free case the steady-state value of x_1 remains constant, that is, $\dot{x}_1 = 0$. This is only possible if the signal ($-\beta x_1$) at the input of the x_1 integrator is exactly compensated by a static phase error such that

$$-\beta x_1 + (1 - 2\zeta\beta + \beta^2) \sin \phi_s = 0. \quad (41)$$

As long as $x_1 \leq \Delta\omega/\omega_n < 1/\beta$ (hold-in range) the loop remains in lock.

If, due to noise, the loop slips a cycle, there exists a random difference $(\Delta\omega/\omega_n) - x_1$ after completion of the slip. A necessary condition for the PLL to resume lock is that it is capable of reducing this difference to zero, on the average. This might require a long pull-in period involving many cycle slips.

Mathematically, this condition requires that the average pull-in voltage $\overline{\sin \phi}$ for a given difference $(\Delta\omega/\omega_n) - x_1$ must be larger in amplitude than the decay βx_1 of the leaky integrator.

$$\overline{\sin \phi} \geq \beta x_1. \quad (42)$$

Otherwise, the value of x_1 decays to zero and the PLL falls out of lock forever, as has been the case in Fig. 16.

The worst case occurs for large frequency differences $(\Delta\omega/\omega_n) - x_1$. In this case we may use the result of (29) if we replace x_1 by $x_1 - \Delta\omega/\omega_n$. Then for $\Delta\omega > 0$ we obtain

$$\overline{\sin \phi} = \frac{\zeta}{\Delta\omega/\omega_n - x_1} \geq \beta x_1 \quad (43)$$

or slightly rearranged

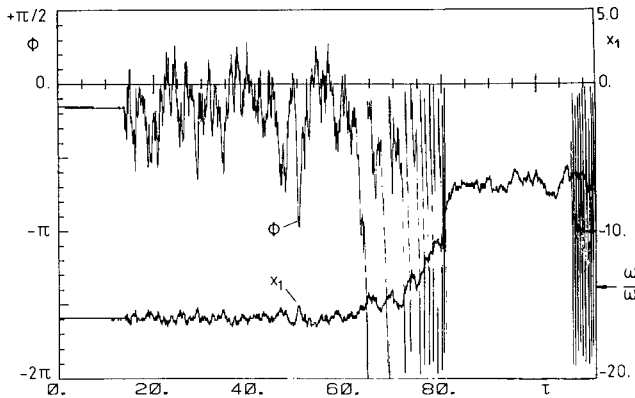


Fig. 16. Trajectories $\phi(\tau)$ and $x_1(\tau)$ for the same parameters as in Fig. 15, but for $\Delta\omega/\omega_n = 16$. The loop starts with correct initial conditions at $\tau = 0$ and drops lock after first slip.

$$x_1^2 - (\Delta\omega/\omega_n)x_1 + \zeta/\beta \geq 0. \tag{44}$$

In general, for a given $\Delta\omega/\omega_n$ and ζ/β , there exists an interval of x_1 for which the inequality is not true. If the loop slips a cycle and x_1 accidentally assumes a value in this interval, resuming lock would be purely by chance. Such behavior is clearly unacceptable in a practical application. The question arises whether there are values of $\Delta\omega/\omega_n$ and ζ/β for which the quadratic form (44) is positive for all values of x_1 . Then, the loop could always reduce the difference $(\Delta\omega/\omega_n) - x_1$ to zero.

Indeed, the quadratic form is strictly positive if the discriminant is negative.

$$(\Delta\omega/\omega_n)^2 - 4\zeta/\beta < 0 \tag{45}$$

or

$$\Delta\omega/\omega_n < 2 \sqrt{\frac{\zeta}{\beta}}. \tag{46}$$

But the right-hand side of (46) is nothing but the pull-in frequency ω_p/ω_n ; see (24).

In conclusion, the loop must be designed such that $|\Delta\omega/\omega_n|$ is sufficiently smaller than the pull-in frequency ω_p ; this is particularly important for low SNR's. From (46) one concludes that a perfect integrator ($\beta = 0$) realized by means of an active loop filter is preferable. In practice, however, due to ever present drift currents, there will always be a limit on the maximum permissible frequency difference.

For the ratio between positive and negative cycle slips, the following formula valid for a first-order loop has been derived:

$$\frac{N+}{N-} = \exp\left(\frac{\pi}{2} \rho \frac{\Delta\omega}{B_L}\right). \tag{47}$$

In any case, the sum

$$N = N_+ + N_- \tag{48}$$

is always greater for $\Delta\omega \neq 0$ than for no loop detuning [2].

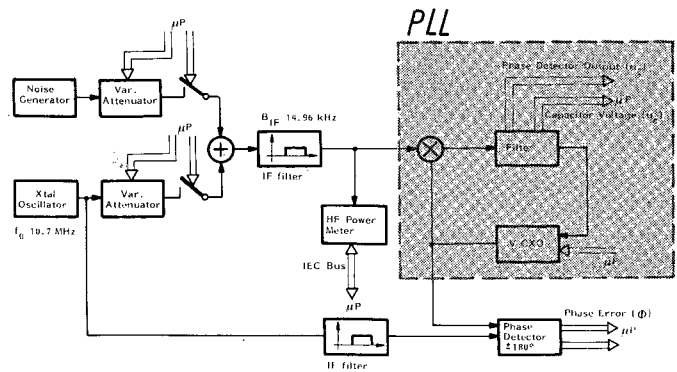


Fig. 17. Simplified block diagram of experimental configuration.

IV. EXPERIMENT

A. Experimental Configuration

The configuration is divided into two parts, the experiment itself, in analog hardware, and a microprocessor (μP) system for control of parameters and recording of measured data. In this section, a survey of the hardware and a functional description of the μP system, based on a Z80 CPU, will be given. For a more detailed discussion see [6].

A block diagram of the analog hardware is shown in Fig. 17. An unmodulated carrier is provided by a crystal (Xtal) oscillator. The signal power can be set by a variable attenuator. Wide-band Gaussian noise from a random noise generator is added. The noise power can be varied by a second attenuator. Both signal and noise may also be switched off.

Filtered by the IF quartz filter, the noise becomes a narrow-band Gaussian process as described in Table I. At the output of the filter, the signal and the noise power are measured. The filter output is also the input to the phase detector of the PLL.

The phase detector is of the multiplier type, the only one usable at low SNR. The passive loop filters are exchangeable. The VCO output is not only connected to the loop phase detector, but also to a reference phase detector.

The undisturbed carrier is directed along a reference path to the other input of this linear $\pm 180^\circ$ phase detector to determine the actual phase error $\phi(t)$. A second quartz filter has been inserted into the reference path, adjusted to compensate for the phase shift of the IF filter.

The connections between the analog hardware and the μP system are marked by double lines in Fig. 17. The μP sets the variable attenuators in steps of approximately 0.05 dB/bit. The center frequency of the VCO is adjusted by a digital-to-analog converter.

The digital power meter is connected to the μP system by an IEC-bus. Thus, the μP can not only read off values from the power meter, but also send commands to the power meter, such as zero calibration and mode commands. If the power is measured in dB_m , a four digit value results, with a least significant digit of $1/100 \text{ dB}_m$.

Three analog-to-digital converters, all buffered by sample and hold amplifiers, allow the μP system to record values of the phase detector output of the PLL (u_0), the capacitor voltage (u_c) of the loop filter of the second-order PLL, and the actual phase error ϕ .

In addition, the output of the reference phase detector is connected to a cycle slip detector, which provides a signal to the μP whenever the phase error exceeds a value of 2π . By means of a second signal the direction of the cycle slips to the μP system is recorded.

The μP system and the analog hardware are strictly separated to avoid signal interference. The analog hardware is built into a shielded box with separate voltage supply. In addition, the analog hardware itself is again built in five subblocks shielded individually to avoid internal interference. These are signal path, noise path, IF path, reference path, and the PLL.

The function of the μP system in the measurement are

- 1) zero calibration of the power meter,
- 2) signal and noise power setting,
- 3) VCO center frequency adjustment,
- 4) sampling and storing of the measured data during measurement, and
- 5) frequent recalibration in measurements of long duration.

The actual parameters and the measured data are stored together in a random access memory (RAM). The stored parameters are the measured signal and noise power, a filter identifier, the digital-to-analog converter values, the offset of phase detector output (u_0), and capacitor voltage (u_c).

The microprocessor system is connected to a larger machine (PDP 11/60) for two purposes.

- 1) different types of measurement programs can be loaded from the PDP to the μP system, which gives high flexibility.
- 2) after completion of a measurement the contents of the random access memory are sent to the PDP for processing, such as evaluation of statistics or graphical display.

The main advantages of the microprocessor control may be mentioned here. As the actual parameters are stored together with the measured data, confusion of different measurements or erroneous readings of the parameters are avoided. The fact that the attenuators can only adjust discrete power levels has no influence on the accuracy of the measurement, as only the actual parameters are used for the evaluation of the statistics.

Furthermore, it is advantageous that long-time measurements are also possible. Some numerical examples of the duration of a complete measurement are given in Table II. An equivalent loop bandwidth of $B_L = 750$ Hz is assumed for the computations. In the described configuration, this value can not be exceeded very much, since it still has to be much smaller than the IF filter bandwidth $B_{IF} = 14.96$ kHz. Displayed in Table II are the mean time between cycle slips $E(T_S)$ and the mean duration of a complete measurement $E(T_M)$ for a few values of $E(B_L T_S)$.

$E(T_M)$ is computed for 1600 events to be recorded, which is the maximum number that can be stored in the RAM, and an arbitrary chosen minimum of 300 events to be recorded. As can be seen, the mean duration of the experiment increases rapidly and for $E(B_L T_S) = 10^8$ an unacceptable duration results. Besides, the results will not be reliable for such low rates.

If higher rates of $E(B_L T_S)$ are supposed to be measured, the duration of the experiment can only be shortened by increasing the equivalent loop bandwidth B_L . On the other hand, this decreases the minimum distance between cycle slips

TABLE II
MEAN DURATION OF AN EXPERIMENT $E(T_M)$

$B_L = 750$ Hz $E[B_L T_S]$	$E[T_S]$	$E[T_M]/1.600$ events	$E[T_M]/300$ events
10^1	13.3 ms	21.3 s	
10^5	133.3 s	60 h	11 h
10^8	37 h		463 days

at lower signal-to-noise ratios. But the minimum distance that can be recorded with the described configuration is limited by the speed of both the analog-to-digital converters and the μP system.

Another aspect has to be taken into consideration at higher signal-to-noise ratios. The mean time between slips increases exponentially with ρ . Assume the bandwidth B_{IF} is measured with x percent uncertainty. The computed value of ρ (see Table I) will have the same uncertainty. The slip rate will have an uncertainty proportional to $\exp(\rho x/100)$.

An exponential dependence of ρ will lead to an increasing asymmetry in the distribution of the direction of the cycle slips if the phase detector is not symmetrical to phase error $\phi = 0$ or if the VCO gain is not symmetrical for positive and negative detuning.

With the described configuration, measurements of the slip rate of a first-order loop, where analytical results exist, were made. In the range $10^{0.5} < E(B_L T_S) < 10^5$ excellent agreement occurred (see Fig. 18). At low rates, a degradation appears due to the limiting of the noise within the phase detector. At higher rates the duration of the measurement is too long.

B. Results

The distribution $P(T_S < t)$ was found to be very nearly exponential for sufficiently large damping factors and signal-to-noise ratios:

$$P(T_S < t) = 1 - \exp(-t/E(T_S)). \quad (49)$$

The mean time $E(T_S)$ between slips versus ρ is displayed in Fig. 18.

For small damping factors, a significant departure from the exponential distribution is visible for very small t ; see Fig. 7 for a typical example. This feature must be attributed to bursting of the slips.

If we exclude all slips occurring very shortly after a predecessor, the conditional probability that $T_S < t$ under the condition that T_S exceeds t_0 results in

$$P[T_S < t | T_S > t_0]. \quad (50)$$

Using Bayes' rule it yields

$$P[T_S < t | T_S > t_0] = \frac{P(T_S < t) - P(T_S < t_0)}{1 - P(T_S < t_0)}. \quad (51)$$

The conditional distribution describes the statistics between bursts, rather than slips. As expected, (51) is practically indistinguishable from an exponential distribution (Fig. 7).

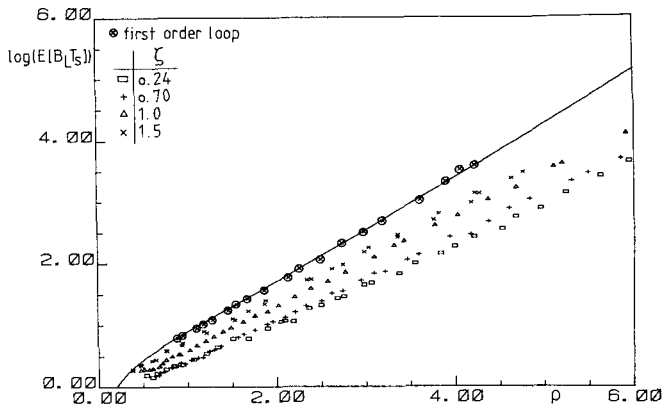


Fig. 18. Normalized mean time between slips of a second-order PLL as a function of ρ with ζ as parameter. Zero loop detuning. Solid line shows analytical results for first-order PLL.

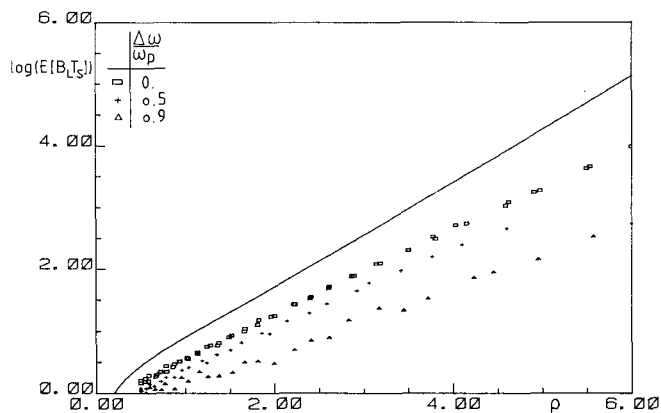


Fig. 19. Normalized mean time between slips of a second-order PLL ($\zeta = 1.0$; $\beta = 0.03$) with loop detuning $\Delta\omega$ normalized to the pull-in frequency ω_p .

The effect of loop detuning on $E(T_s)$ is shown in Fig. 19. The frequency difference $\Delta\omega$ is normalized to the pull-in frequency ω_p .

The importance of the state variable x_1 has been discussed at length in this paper.

A key finding of this paper has been the behavior of x_1 immediately following a slip; a consistent departure from the correct value has been identified. The statistics of the conditional means $E[x_1 | \phi = \pm 2\pi]$ and variance $E[(x_1 - E(x_1))^2 | \phi = \pm 2\pi]$ can be found in Fig. 9.

A typical distribution of x_1 immediately following a slip is displayed in Fig. 20 for $\zeta = 0.7$. As a consequence of the occurrence of bursts a significant skewness is visible. If one excludes the very short time interval between slips from consideration, the skewness disappears and both sides of the distribution assume a symmetrical shape.

C. Optimum Loop Parameters

The usual approach in designing a PLL uses linear theory to determine the loop parameters for a given set of specifications. For the next step, if necessary, the slip rate for the resulting parameters can be obtained from Fig. 18 and checked against a specified maximum permissible number for the particular application.

For certain applications, it is of interest to optimize the loop parameters to achieve maximum mean time between

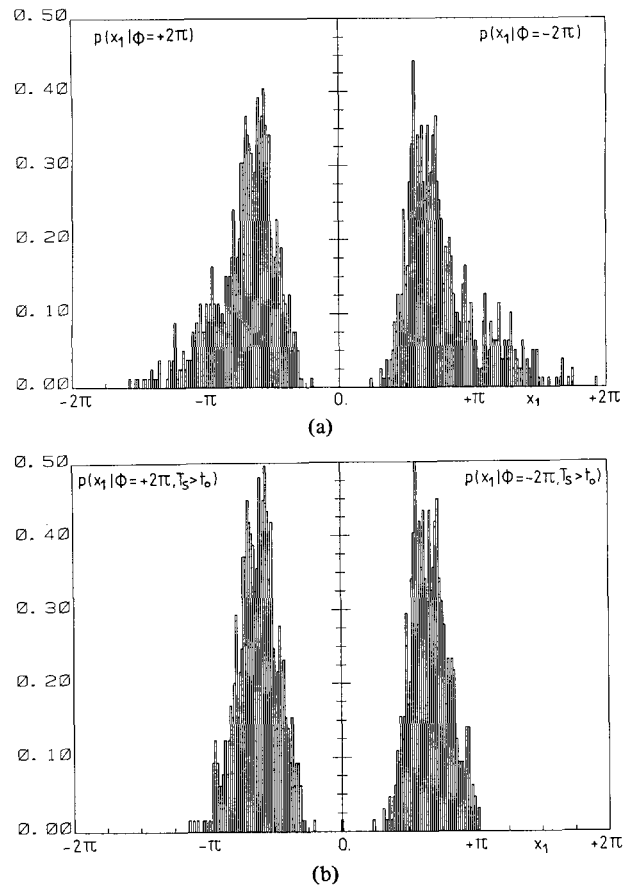


Fig. 20. (a) Experimentally derived conditional probability density function $p(x_1 | \phi)$ for a second-order loop with $\zeta = 0.7$ and $\rho = 2.1$. (b) Conditional probability density function $p(x_1 | \phi, T_s > t_0)$ obtained if slips of duration T_s shorter than $t_0 \ll E(T_s)$ are excluded ($E(T_s)/t_0 = 43.5$).

cycle slips. Such an optimization is a formidable task that can be carried out only numerically on a digital computer or in the form of an experiment.

In a second-order loop there are essentially two loop parameters, namely bandwidth B_L and loop damping ζ , to be optimized in a two-dimensional search. The loop parameters have to be clearly distinguished from the signal parameters $\{P_s, N_0, \Delta f\}$ which are fixed quantities. In a first step we want to optimize the loop bandwidth B_L for a given damping ζ . For this purpose we seek a suitable normalized representation of the mean time between cycle slips $E(T_s)$ as a function of the bandwidth B_L . It is natural to modify the familiar plot of normalized mean time between slips $E[B_L T_s]$ versus ρ as depicted in Fig. 19.

The signal-to-noise ratio is a function of the two signal parameters P_s, N_0 , and the loop parameter B_L :

$$\rho = \frac{P_s}{N_0} \frac{1}{B_L} \tag{52}$$

If we multiply both numerator and denominator by Δf we obtain instead of (52)

$$\rho = \frac{P_s}{N_0 \Delta f} \frac{\Delta f}{B_L} \tag{53}$$

The three signal parameters can be grouped into a single quantity b :

$$b = \frac{N_0 \Delta f}{P_s} \quad (54)$$

which is related to the loop parameters γ and ρ as follows:

$$\rho = (1/b)\gamma \quad (55)$$

with

$$\gamma = \frac{\Delta f}{B_L}: \quad \text{normalized loop stress.} \quad (56)$$

From (55) we learn that for plotting $E[B_L T_s]$ versus ρ either the signal parameter b can be kept constant and γ varied or vice versa. The two possibilities lead to different sets of curves: the case where a fixed relative offset $\Delta f/B_L$ is maintained is depicted in Fig. 19 (with a different normalization), while in Fig. 21 we have plotted the curves for a constant b on a double-logarithmic scale.

The dashed curves in Fig. 21 display $E[B_L T_s]$ for a first-order loop where an analytical formula exists [2]:

$$E[B_L T_s] = \frac{\rho}{2} \frac{\pi^2 |I_{j\gamma\rho}(\rho)|^2}{\cosh(\pi\gamma\rho)}; \quad b = \frac{N_0 \Delta f}{P_s} = \text{const.} \quad (57)$$

The maximum in these curves is qualitatively easily understood. A small ρ implies a large bandwidth B_L :

$$\rho = \frac{1}{b} \frac{\Delta f}{B_L} \quad (58)$$

resulting in a large number of slips due to poor noise suppression. For increasing ρ , the bandwidth is decreased and the loop slips less cycles. If, however, the bandwidth is decreased beyond the optimum, the static phase error caused by Δf starts to interfere and the mean time between slips starts to increase again. The smaller b is, the smaller the optimum bandwidth; in the limiting case for $b = 0$ we obtain a strictly increasing curve. The curves labeled with \square and $+$ are experimental results for a second-order loop with $\zeta = 1.0$ and $\beta = 0.03$.

Because the normalized quantity $\log(E[B_L T_s])$ is displayed in Fig. 21 [and not $E(T_s)$] the optimum B_L is not found at the location of the maximum of these curves. We will show below how the optimization can be carried out by means of a graphic procedure.

Multiplying numerator and denominator of ρ by $E(T_s)$ (11) and taking the logarithm yields

$$\log \rho = \log \left(\frac{P_s}{N_0} E(T_s) \right) - \log E[B_L T_s] \quad (59)$$

or rearranged

$$\log E[B_L T_s] = -\log \rho + \log \left(\frac{P_s}{N_0} E(T_s) \right). \quad (60)$$

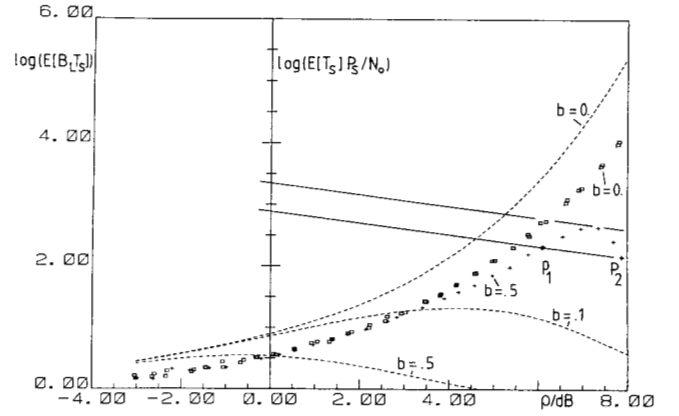


Fig. 21. Analytically derived mean time between slips for first-order loop (dashed curves) and experimental results for second-order loop ($\zeta = 1.0$; $\beta = 0.03$) with $b = \Delta f/(P_s/N_0)$ as parameter.

For any given $E(T_s)$, (60) represents a straight line in Fig. 21; with increasing $E(T_s)$ the line moves upwards.

Let us assume that such a line intersects a curve $\log(E[B_L T_s])$ as illustrated for $b = 0.5$, and let us label the point of intersection P_1 , and the corresponding ρ by ρ_{i1} . Solving (58) for B_L yields

$$B_{L1} = \frac{\Delta f}{\rho_{i1} b} \quad (61)$$

which determines the bandwidth of the loop for a given $E(T_s)$ and parameters ρ_1 and b . In our example the line also intersects the same curve at the point P_2 . This means that the same mean time between slips is obtained for two different loop bandwidths.

If we now increase $E(T_s)$, then according to (60) the straight line moves upwards until the two points P_1 and P_2 finally converge to one point defined as the tangent of the curve with the slope given by (60). Since for values of $E(T_s)$ above that point no intersection exists, we have found the maximum achievable $E(T_s)$ for any loop bandwidth. Therefore, the optimum bandwidth for a given signal parameter b can be found by constructing the tangent to the particular curve. In Fig. 22 we have plotted $\log(E[B_L T_s])$ as a function of ρ for the two damping factors $\zeta = 0.7$ and $\zeta = 1.0$. We observe a slow increase up to the maximum and a steep descent beyond the optimum. As expected, the loop with the larger damping performs better. For $b = 0$ the function $\log(E[B_L T_s])$ increases monotonically. In theory, any desired $E(T_s)$ can thus be obtained with a sufficiently narrow loop bandwidth. We also see that the first-order loop always performs better than the second-order loop for $b = 0$ (but compare the two loops for $b = 0.5$). This is not surprising. For zero frequency detuning, the integrator in the loop filter is superfluous, only causing additional slips by feigning a loop stress.

Our discussion on optimal loop parameters is brief and incomplete. A more detailed discussion can be found in [7]. It was found in this study that the loop parameters for maximum $E(T_s)$ were distinctly different from those obtained via linear Wiener filtering theory. In particular, the favorite $\zeta = 0.707$ was found to be too small; a better choice is $\zeta = 1.0$ - 1.2 .

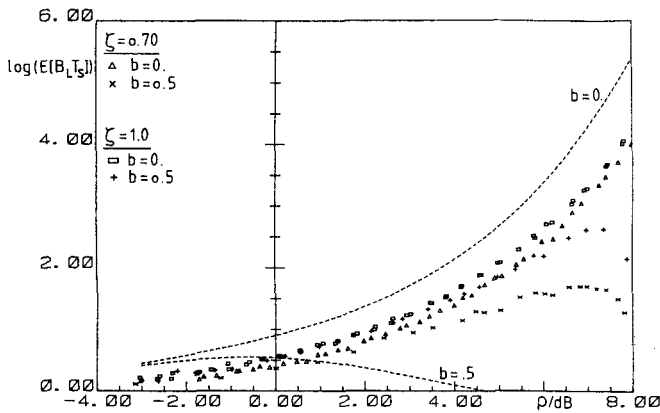


Fig. 22. Experimental mean time between cycle slips for second-order loop for $\zeta = 1.0$ and $\zeta = 0.7$ ($\beta = 0.03$) with b as parameter.

V. SUMMARY AND CONCLUSIONS

Cycle slips in phase-locked loops are statistical, nonlinear phenomena. The complicated interaction of nonlinearity and noise has been described. Experimental results were complemented by simple analyses to obtain a quantitative understanding of the influence of the various signal/loop parameters on cycle slip statistics.

It has been shown that a state variable representation is needed to discuss cycle slips properly. Besides the phase error, which is defined in a $\pm 2\pi$ interval according to the definition of a slip (and not modulo 2π), the state variable x_1 plays a central role. This fact, which has not received proper attention in the older literature, was first discussed in several theoretical papers; see [8], [9].

From a theoretical point of view it is interesting to observe that the experimentally determined mean time between slips for a first-order loop perfectly agrees with the results obtained via Fokker-Planck technique (which assumes a white noise process).

ACKNOWLEDGMENT

We have greatly profited from the expertise of Dr. F. Gardner who spent freely of his time to review the manuscript. His detailed critique made the paper better than it would have been without his help. We would also like to acknowledge the constructive criticism made by Mrs. McKenzie, Dr. W. Braun, and Dr. C. Chie of LinCom and L. Popken of RWTH Aachen.

The support of the Deutsche Forschungsgemeinschaft (DFG) is greatly appreciated.

REFERENCES

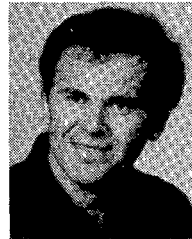
[1] W. C. Lindsey and M. K. Simon, *Telecommunication Systems Engineering*. Englewood Cliffs, NJ: Prentice-Hall, 1973.
 [2] W. C. Lindsey, *Synchronization Systems in Communication and Control*. Englewood Cliffs, NJ: Prentice-Hall, 1972.
 [3] A. J. Viterbi, *Principles of Coherent Communications*. New York: McGraw-Hill, 1966.
 [4] A. Blanchard, *Phase-Locked Loops. Application to Coherent Receiver Design*. New York: Wiley, 1978.

[5] F. M. Gardner, *Phaselock Techniques*. New York: Wiley, 1979.
 [6] G. Ascheid and H. Meyr, "Microprocessor-controlled experiment to determine cycle slip statistics: Hardware and software." *ERT-Rep.* 713/18, Sept. 1981.
 [7] —, "Parameter optimization in PLLs: An experimental study," *ERT-Rep.* 713/19, Sept. 1981.
 [8] W. C. Lindsey and H. Meyr, "Complete statistical description of the phase-error generated by correlative tracking systems," *IEEE Trans. Inform. Theory*, vol. IT-23, pp. 794-802, Mar. 1977.
 [9] D. Ryter and H. Meyr, "Theory of phase tracking systems of arbitrary order: Statistics of cycle slips and probability distribution of the state vector," *IEEE Trans. Inform. Theory*, vol. IT-24, pp. 1-7, Jan. 1978.
 [10] F. J. Charles and W. C. Lindsey, "Some analytical and experimental phase-locked loop results for low signal-to-noise ratios," *Proc. IEEE*, vol. 54, pp. 1152-1166, Sept. 1966.
 [11] R. W. Sannemann and J. R. Rowbotham, "Unlock characteristics of the optimum type II phase-locked loop," *IEEE Trans. Aerosp. Navig. Electron.*, vol. ANE-11, pp. 15-24, Mar. 1964.
 [12] R. C. Tausworthe, "Cycle slipping in phase-locked loops," *IEEE Trans. Commun. Technol.*, vol. COM-15, pp. 417-421, June 1967.
 [13] W. C. Lindsey and R. C. Tausworthe, "A bibliography of the theory and application of the phase-lock principle," *Jet Propulsion Lab., Pasadena, CA, Tech. Rep.* 32-1581, Apr. 1, 1973.
 [14] "Statistical loop analyzer (SLA)," *LinCom Tech. Rep.*, Mar. 1982.



Gerd Ascheid was born in Cologne, Germany, on June 14, 1951. He received the Dipl.-Ing. degree from the Technical University of Aachen (RWTH Aachen), Germany, in 1978.

He is now a Research Assistant at the Department of Electrical Engineering, RWTH Aachen, working toward the Ph.D. degree. His main interest is in synchronization, especially of bandwidth-efficient modulations.



Heinrich Meyr (M'75) received the Dipl.-Ing. and Ph.D. degrees from the Swiss Federal Institute of Technology (ETH), Zurich, Switzerland, in 1967 and 1973, respectively.

From 1968 to 1970 he held research positions at Brown Boveri Corporation, Zurich, and the Swiss Federal Institute for Reactor Research. From 1970 to the summer of 1977, he was with Hasler Research Laboratory, Bern, Switzerland, doing research in the fields of digital facsimile encoding and tracking systems. His last position at Hasler was manager of the Research Department. During 1974 he was a Visiting Assistant Professor with the Department of Electrical Engineering, University of Southern California, Los Angeles. Since the summer of 1977 he has been a Professor of Electrical Engineering at the Aachen Technical University (RWTH Aachen), Germany. His research interests include synchronization, estimation, and, in particular, the interaction of implementation issues, and the design of control and estimation/measurement systems. Presently he is consultant to the IBM Research Laboratory, Zurich, in the area of synchronization of local area computer networks and to Krohne Ltd., Duisburg, Germany, in the area of digital signal processing. He has published work in various fields and journals and holds over a dozen patents.

Dr. Meyr served as a Vice Chairman for the 1978 IEEE Zurich Seminar and as an International Chairman for the 1980 National Telecommunications Conference, Houston, TX. He presently serves as Associate Editor for the IEEE TRANSACTIONS ON ACOUSTICS, SPEECH, AND SIGNAL PROCESSING.